Structure and Dynamics of Potassium Chloride in Aqueous Solution

Structure and Dynamics of Potassium Chloride in Aqueous Solution

Julien O. Sindt, Andrew J. Alexander, and Philip J. Camp*

School of Chemistry, University of Edinburgh, West Mains Road, Edinburgh EH9 3JJ, Scotland

E-mail: philip.camp@ed.ac.uk

July 14, 2014

*To whom correspondence should be addressed

Abstract

The structure and dynamics of potassium chloride in aqueous solution over a wide range of concentrations – and in particular beyond saturation – are studied using molecular-dynamics simulations to help shed light on recent experimental studies of nonphotochemical laser-induced nucleation (NPLIN). In NPLIN experiments, the duration, t, of the laser pulse (with wavelength 1064 nm) is found to influence the occurrence of crystal nucleation in supersaturated KCl(aq): if t is less than about 5 ps, no crystal nucleation is observed; if t is greater than about 100 ps, crystal nucleation is observed, and with a known dependence on laser power. Assuming that the laser acts on spontaneously formed solute clusters, these observations suggest that there are transient structures in supersaturated solutions with relaxation times on the scale of 5–100 ps. Ion-cluster formation and ion-cluster lifetimes are calculated according to various criteria, and it is found that, in the supersaturated regime, there are indeed structures with relaxation times of up to 100 ps. In addition, the ion dynamics in this regime is found to show signs of collective behavior, as evidenced by stretched exponential decay of the self-intermediate scattering function. Although these results do not explain the phenomenon of NPLIN, they do provide insights on possible relevant dynamical factors in supersaturated aqueous solutions of potassium chloride.

Keywords: clusters, crystallization, KCl, molecular dynamics, nonphotochemical laser-induced nucleation

1 Introduction

The structure and dynamics in aqueous electrolyte solutions are important in a vast range of situations in chemistry, biochemistry, and chemical engineering.[1] For example, the phenomenon of electrostatic screening by ions in solutions underpins colloidal stability and (bio)macromolecular interactions,[2] and the structural organization and dynamics of ions near interfaces are central to electrochemistry.[3] Needless to say, immense research effort has been expended on developing detailed microscopic models of aqueous electrolyte solutions using theory and computer simulation. This work is focused on aqueous solutions of potassium chloride (KCl), particularly in the supersaturated regime, and is motivated by recent experiments on nonphotochemical laser-induced nucleation (NPLIN).

NPLIN is the phenomenon by which incident laser light causes the crystallization of solute from a supersaturated solution. Typical laser variables include the wavelength, pulse duration, polarization, and intensity. The effect was discovered by Garetz *et al.* in 1996.[4] It was observed that 20 ns pulses of linearly polarized near infrared (NIR) light of wavelength $\lambda = 1064$ nm and total energy ~ 0.1 J incident upon supersaturated aqueous solutions of urea gave elongated urea crystals oriented along the laser polarization axis. This was thought to arise from a nonlinear optical Kerr effect, where molecules within an existing precritical cluster align due to the molecular polarizability anisotropy; this alignment would then result in a crystalline arrangement of solute molecules, and the cluster would become a viable crystal nucleus. The role of laser polarization was demonstrated most vividly in NPLIN experiments on glycine solutions.[5,6] It was found that, in certain ranges of supersaturation where α-glycine nucleates spontaneously, linearly and circularly polarized laser pulses produced the γ and α polymorphs, respectively; γ-glycine is the thermodynamically stable solid phase. These trends can again be correlated with the molecular polarizability anisotropy of the molecules, and the way that the molecules pack in the different polymorphs: in α-glycine, the molecules are arranged in double planes of cyclic dimers, leading to disk-like polarizability; in γ-glycine, the molecules are ordered more helically, corresponding to rod-like polarizability. Crystal nucleation is an extremely complicated phenomenon, and in

combination with light-matter interactions, it becomes even more difficult to study.

In order to understand the ultimate origins of NPLIN, it is vital to study simple systems. To this end, Alexander and coworkers have embarked on a program of systematic experiments on simple solutes in aqueous solution. To date, the most chemically simple system in which NPLIN can be demonstrated is potassium chloride in aqueous solution.[7–9] Supersaturated KCl(aq) solutions can be prepared at ambient temperatures ($20-23^{\circ}$ C) that remain metastable for periods of up to months. Recently, Fang *et al.* have demonstrated NPLIN in levitated droplets of supersaturated KCl(aq), which shows that this is a bulk phenomenon, and not associated with the macroscopic surface of the container.[10] Quoting from ref 7, there are two more important observations to be made about NPLIN in KCl(aq). "1. Significant periods (hours or days) of aging of the supersaturated solutions are not required. 2. Nucleation of a single crystal of KCl can be induced with a single laser pulse, whereas urea and glycine required hundreds of shots over tens of seconds." In ref 7 the probability of crystal nucleation was examined as a function of laser intensity and supersaturation. It was found that there is a laser threshold intensity below which NPLIN is not observed. The origin of this threshold is unknown. Above the threshold, the increase in nucleation probability with increasing laser intensity could be described quantitatively by assuming that the electric field of the laser electronically polarizes existing subcritical KCl clusters, hence reducing their bulk free energy with respect to the surrounding solution, and rendering a proportion of them supercritical crystal nuclei. This polarization effect can be incorporated in to a standard classical nucleation theory (CNT) calculation, and the dependence of the nucleation probability on variables such as supersaturation, temperature, (frequency-dependent) dielectric properties of the solute, laser wavelength, and laser intensity can be rationalized. One of the outstanding problems, however, is the fact that CNT predicts that the nucleation probability should increase in direct proportion to the laser intensity, while in experiments there is the threshold [and not only with KCl(aq)]. Full details of the "dielectric" CNT are given in ref 7 but it has been applied successfully – threshold notwithstanding – to KCl trapped in gels,[8] and to other potassium halide solutions where the variations of nucleation probability with solute dielectric properties, laser wavelength, and temperature were

explored systematically.[11] Nonetheless, the model cannot be entirely correct. Firstly, a subcritical cluster is idealized as a spherical dielectric cavity immersed in a dielectric continuum. Secondly, the model does not explain the existence of a threshold laser intensity.

In an initial study of the effects of pulse duration, it was found that the nucleation probability in KCl(aq) is the same for NIR laser-pulse durations of 6 ns and 200 ns with equivalent peak intensities.[9] In as-yet unpublished work, Alexander and co-workers have explored the dependence of the nucleation probability on shorter laser-pulse durations. The key result is that with laser pulses of less than about 5 ps, NPLIN is not observed irrespective of intensity, while with a pulse duration of more than about 100 ps, NPLIN is observed and with the dependence on laser intensity found in the earlier work using longer pulse durations.

There is growing experimental, theoretical, and simulation support for two-step nucleation scenarios for a broad range of systems.[12–14] In such a scenario, nucleation proceeds not only by growth of a cluster, but also by structural reorganization of the cluster: in other words, several order parameters may be required to describe the progress of a nucleating cluster along a reaction coordinate. One version of two-step nucleation may therefore consist of the growth of an amorphous cluster, followed by structural reorganization, and each of these processes may be impeded by free-energy barriers. Of particular relevance to the current work is that *homogeneous* nucleation in simulated aqueous sodium chloride solutions occurs via a two-step mechanism, in which the formation of a disordered, ion-rich region is followed by structural ordering to form a critical nucleus (of roughly 1 nm diameter and containing around 75 ions).[15,16] In other computational work on NaCl solutions, so-called "transient polymorphism" has been observed in metadynamics simulations, in which wurtzite-like structures are found to nucleate in preference to the rocksalt structure.[17] NPLIN in NaCl(aq) has not yet been demonstrated due to experimental difficulties: the solubility of NaCl is only weakly dependent on temperature, and so it is difficult to form highly supersaturated solutions without cooling below ambient temperature, which is inconvenient.

Continuing with the two-step nucleation theme, if the basic mechanism of NPLIN involves the direct interaction of light with existing solute clusters that somehow promotes the formation of vi-

able crystal nuclei, then perhaps there are dynamical signatures on the right timescales corresponding to structural reorganization of amorphous solute clusters. To this end, molecular-dynamics (MD) simulations could offer some useful information. Two essential points need to be made here. Firstly, NPLIN *cannot* yet be simulated directly using MD simulations, because the basic action of the laser pulse on the supersaturated solution is unknown. Secondly, although there is a huge simulation literature on homogeneous and heterogeneous nucleation, this is not relevant to the current problem. The technical demands of simulating rare events such as homogeneous crystal nucleation are well known, but in the present case, the low nucleation rates in finite-size systems can be of help: it is the structure of the metastable supersaturated solution that is of interest here, and homogeneous crystal nucleation on the simulation timescale is to be avoided. Indeed, even in experiments, supersaturated KCl solutions do not reach the solid region of phase space for several months! So, the aim of this work is to characterize the structure and dynamics of KCl in aqueous solution across a wide range of concentrations, and particularly above saturation. Although the interaction between simple ions and water must be critical for phenomena such as crystalloluminescence,[18,19] here the focus is on whether the ions form transient clusters, and if so, for how long; the dynamics of the hydration shell is considered only very briefly.

This article is organized as follows. In Section 2, the KCl(aq) models and the MD simulation protocol are defined. The results are presented in Section 3, which begins with a critical analysis of the molecular models by comparison of the simulated mass density, molar conductivity, and ion self-diffusion coefficients with experimental data. Then, the structures of KCl(aq) solutions ranging from low concentration to high supersaturation are characterized using radial distribution functions and structure factors. Next, the degree of ion association and cluster-size distribution are computed, and the associated lifetimes are identified by calculating appropriate time-correlation functions. Hydration of the ions and the associated residence times are considered briefly. Space-dependent self diffusion of the ions is examined using the self-intermediate scattering function, and evidence for collective behavior in the supersaturated regime is presented. Finally, in Section 4, all of these results are drawn together to present a picture of the structure and dynamics in

supersaturated KCl(aq), and how these might play a role in the mechanism of NPLIN.

2 Model and methods

The choice of interaction potential is obviously crucial, and so several combinations of ion and water models were tested against experimental data, as explained in Section 3. Water was described using the SPC/E model,[20] and the TIP3P-Ew[21,22] and TIP4P-Ew[21,23] models optimized for use with particle-mesh Ewald summations. The K^+ and Cl^- ions were simulated using the parameters developed by Dang,[24] and the parameters optimized for use with TIP4P-Ew water by Joung and Cheatham (JC).[25,26] The combinations considered in this work are labeled SPC/E+Dang, TIP3P-Ew+Dang, TIP4P-Ew+Dang, and TIP4P-Ew+JC. The interatomic interactions are expressed in terms of the Lennard-Jones (LJ) and Coulomb (C) potentials as functions of the site-site separation r_{ij}.

$$u_{ij}^{\mathrm{LJ}}(r_{ij}) = 4\varepsilon_{ij}\left[\left(\frac{\sigma_{ij}}{r_{ij}}\right)^{12} - \left(\frac{\sigma_{ij}}{r_{ij}}\right)^{6}\right] \quad (1)$$

$$u_{ij}^{\mathrm{C}}(r_{ij}) = \frac{q_i q_j}{4\pi\varepsilon_0 r_{ij}} \quad (2)$$

In the TIP4P-Ew model, the charge on the oxygen is offset from its center.[23] The potential parameters q_i (ion charge), ε_{ii}, and σ_{ii} are summarized in Table 1; the Lorenz-Berthelot mixing rules $\sigma_{ij} = (\sigma_{ii} + \sigma_{jj})/2$ and $\varepsilon_{ij} = \sqrt{\varepsilon_{ii}\varepsilon_{jj}}$ were used throughout. Simulation estimates of the thermodynamic properties of combinations of these different models vary widely. As an example, the simulated molal solubility (or saturation molality), b_{sat}, at $T = 298$ K can vary by an order of magnitude: for the TIP4P-Ew-JC water model, $b_{\mathrm{sat}} = 3.99 \pm 0.04$ mol kg^{-1};[26] the SPC/E+Dang and TIP3P-Ew+Dang water models give $b_{\mathrm{sat}} = 0.53 \pm 0.02$ mol kg^{-1} and $b_{\mathrm{sat}} = 0.49 \pm 0.01$ mol kg^{-1}, respectively;[26] and the experimental value is $b_{\mathrm{sat}} = 4.77$ mol kg^{-1}.[27] Joung and Cheatham recommend against using the TIP3P-Ew+Dang model at high concentrations,[26] but while their TIP4P-Ew-JC model would appear to be the natural choice, it does not reproduce accurately some other

Table 1: Interaction potential parameters for all of the systems considered. q_i is the charge, e is the elementary charge, and ε_{ii} and σ_{ii} are the Lennard-Jones parameters appearing in eq 1.

Model	Species i	q_i / e	σ_{ii} / Å	ε_{ii} / kcal mol^{-1}
SPC/E[20]	O	-0.8476	3.166	0.1553
	H	$+0.4238$	0.000	0.0000
TIP3P-Ew[22]	O	-0.830	3.188	0.102
	H	$+0.415$	0.000	0.000
TIP4P-Ew[23]	O	-1.04844	3.16435	0.162750
	H	$+0.52422$	0.00000	0.000000
Dang[24]	K^+	$+1.00$	3.332	0.100
	Cl^-	-1.00	4.401	0.100
Joung and Cheatham[25,26]	K^+	$+1.00$	2.83306	0.2794651
	Cl^-	-1.00	4.91776	0.0116615

basic experimental properties of concentrated KCl(aq), such as the density, molar conductivity, and ion self-diffusion coefficients. A comparison of different models with available experimental data will be given in Section 3. Fortunately, the apparent clustering and cluster lifetimes are insensitive to the choice of model, as will be shown explicitly in Section 3, and so the simulation results presented below are expected to be reliable.

MD simulations were carried out using LAMMPS.[28,29] In all cases, the system consisted of a total of 2000 water molecules, potassium ions, and chloride ions. Initial configurations were generated with the appropriate molalities in the range 0.139 mol kg^{-1} $\leq b \leq$ 8.96 mol kg^{-1}, as summarized in Table 2. Simulations were conducted in the isothermal-isobaric (NPT) ensemble at either $T = 293$ K or 298 K, and $P = 1$ atm using a Nosé-Hoover thermostat and barostat. The velocity-Verlet integration algorithm was used with a timestep of 1 fs, and the water molecules were kept rigid using the SHAKE algorithm. Run lengths of up to 10 ns were carried out after equilibration. The long-range Coulombic interactions were handled using the particle-mesh Ewald summation with conducting boundary conditions, and the Lennard-Jones interactions were truncated at 12 Å.

Table 2: Solution compositions including the numbers of KCl (74.551 g mol^{-1}) and H_2O (18.0153 g mol^{-1}). Supersaturations $s = b/b_{sat}$ are for the experimental value of $b_{sat} = 4.56$ mol kg^{-1} at $T = 293$ K.[27] n_w indicates the average number of water molecules in the first hydration shell of each type of ion from simulations of the TIP3P-Ew+Dang model at $T = 293$ K.

Mass percent KCl	Molality / mol kg^{-1}	KCl	H_2O	s	$n_w(K^+)$	$n_w(Cl^-)$
1.03	0.139	5	1990	0.0306	7.03	6.73
2.05	0.280	10	1980	0.0615	6.97	6.67
4.05	0.566	20	1960	0.124	6.86	6.55
7.94	1.16	40	1920	0.254	6.68	6.38
12.0	1.83	62	1876	0.402	6.48	6.17
14.0	2.19	73	1854	0.479	6.41	6.10
15.9	2.55	84	1832	0.558	6.29	5.97
18.0	2.95	96	1808	0.646	6.12	5.80
20.0	3.36	108	1784	0.737	6.06	5.74
22.0	3.78	120	1760	0.830	5.93	5.61
23.9	4.22	132	1736	0.926	5.83	5.51
25.5	4.59	142	1716	1.01	5.75	5.43
26.0	4.71	145	1710	1.03	5.70	5.39
28.0	5.21	158	1684	1.14	5.53	5.20
30.1	5.77	172	1656	1.26	5.43	5.10
32.0	6.30	185	1630	1.38	5.54	5.03
34.0	6.90	199	1602	1.51	5.25	4.92
36.0	7.56	214	1572	1.66	5.09	4.75
38.1	8.24	299	1542	1.81	4.96	4.63
40.0	8.96	244	1512	1.96	4.81	4.48

3 Results

3.1 Basic physical properties

The results from MD simulations were first compared to experimental measurements of the mass density ρ,[30] the molar conductivity Λ,[1,31,32] and the cation and anion self-diffusion coefficients D_+ and D_- [33,34] for KCl(aq) at $T = 298$ K over a broad range of concentrations. The conductivity and the ion self-diffusion coefficients were calculated using the appropriate Green-Kubo expressions with the single-particle velocity autocorrelation function $C_v(t) = \langle \boldsymbol{v}(t) \cdot \boldsymbol{v}(0) \rangle$ (calculated separately for cations and anions) and the ion-current correlation function $C_J(t) = \langle \boldsymbol{J}(t) \cdot \boldsymbol{J}(0) \rangle$.

$$D = \frac{1}{3} \int_0^\infty C_v(t) \, \mathrm{d}t \tag{3}$$

$$\Lambda = \frac{1}{3Nk_\mathrm{B}T} \int_0^\infty C_J(t) \, \mathrm{d}t \tag{4}$$

Here, N is the total number of ions, and $\boldsymbol{J}(t) = \sum_{i=1}^{N} q_i \boldsymbol{v}_i(t)$. Figure 1 shows ρ, Λ, D_+, and D_- as functions of the salt concentration, expressed throughout in terms of the molality b (mol kg^{-1}), all at $T = 298$ K.[35] The TIP3P-Ew+Dang model shows the best agreement with experimental data for the mass density (Figure 1a). The SPC/E+Dang and TIP4P-Ew+Dang models underestimate the density, but they show the correct slope with increasing concentration. The TIP4P-Ew+JC model is in good agreement with experimental data above $b = 2.5$ mol kg^{-1}, but underestimates the density at lower concentrations. Figure 1b shows that, at high concentrations, the molar conductivity of each simulation model is below the experimental value. The TIP3P-Ew+Dang and TIP4P-Ew+Dang models are closest to reality, but there is not much to choose between any of the models at high concentration, where the discrepancies between simulation and experimental results are around 50%. Figure 1c and d show that at low concentrations, all of the models involving TIP3P-Ew or TIP4P-Ew water are superior to the SPC/E+Dang model, particularly for the self-diffusion coefficient of Cl^-(aq). At high concentrations, the results for the TIP3P-Ew+Dang and TIP4P-Ew+Dang models are almost indistinguishable and closest to experiment.

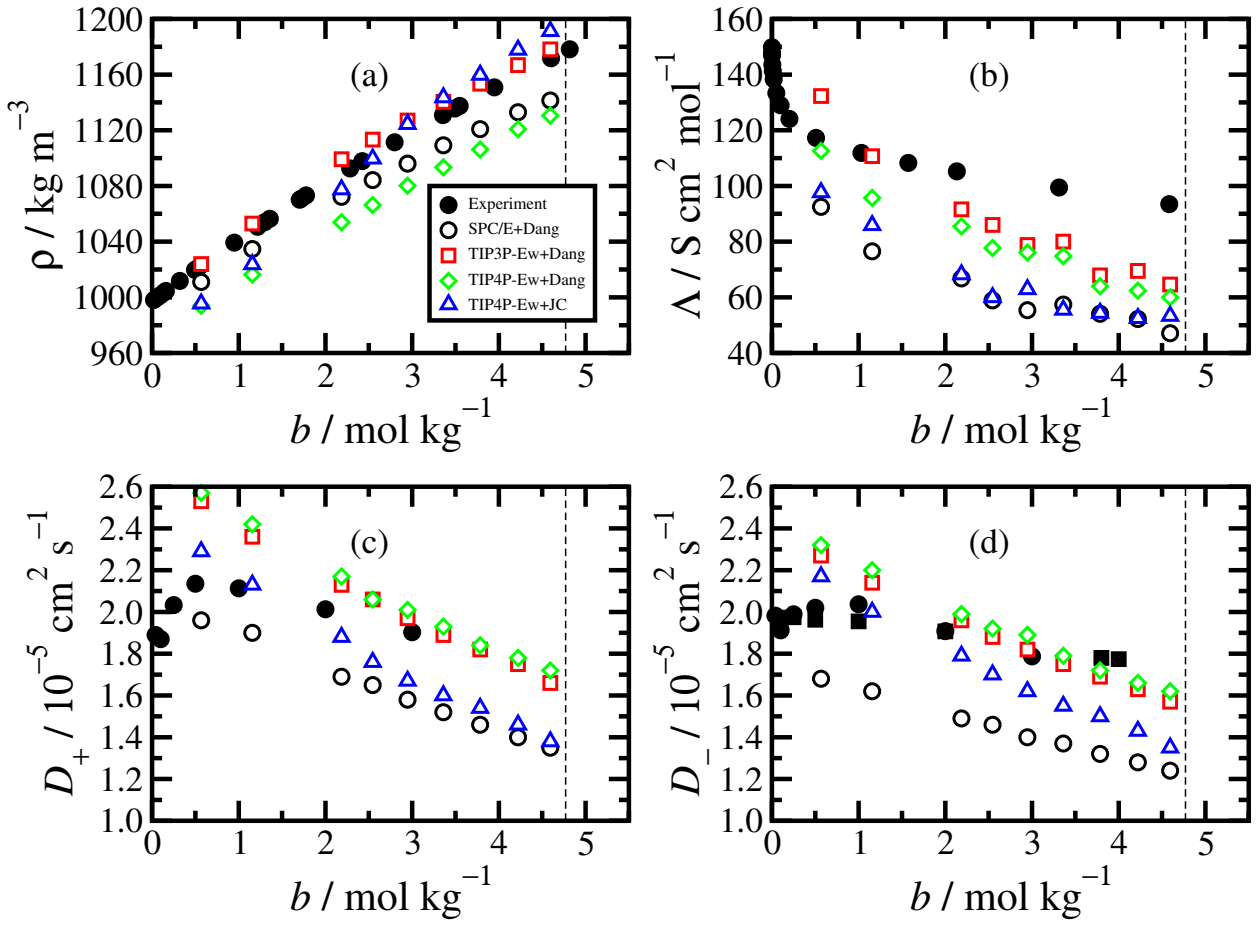

Figure 1: Basic physical properties of KCl(aq) at $T = 298$ K as functions of concentration from simulations with different models (unfilled symbols) and from experiments (filled symbols): (a) mass density;[30] (b) molar conductivity;[1,31,32] (c) and (d) self-diffusion coefficients for K^+(aq)[33] and Cl^-(aq),[33,34] respectively. The vertical dashed lines mark the experimental saturation concentration $b_{sat} = 4.77$ mol kg^{-1} at $T = 298$ K.[27]

The Nernst-Einstein relation links the molar conductivity Λ with the diffusion coefficient of the salt ions $D = D_+ + D_-$, and it is exact at very low concentrations in the limit of independent ion migration. Deviations from the Nernst-Einstein relation can be characterized by a parameter Δ, defined by

$$\Lambda = \frac{F^2 D(1-\Delta)}{RT} \tag{5}$$

where F is Faraday's constant, and R is the molar gas constant. The Nernst-Einstein relation corresponds to $\Delta = 0$. If $\Delta > 0$, then it means that there are ion motions that contribute to diffusion, but do not contribute to the conductivity.[36] One way that this may occur is through (transient) ion association, which will be explored in more detail in Section 3.2. Figure 2 shows Δ as a function of concentration from simulations of each model at $T = 298$ K and $T = 293$ K, and from experimental measurements at $T = 298$ K. The experimental values are calculated from separate measurements of the conductivity[31,32] and the salt diffusion coefficient.[37,38] As expected, Δ rises with increasing concentration, and at around b_{sat}, begins to level off at a value of $\Delta = \frac{1}{2}$. The agreement between the simulation models and experiment closely follows that shown in Figure 1, and overall the TIP3P-Ew+Dang model seems to give the best description.

Overall, the TIP3P-Ew+Dang model gives the best agreement with experiment, and so this model is studied in depth in what follows. Some checks with the TIP4P-Ew+JC model have been carried out, and in all cases, the results do not change significantly. Where this is particularly important, it will be demonstrated explicitly.

3.2 Structure

All of the following results are at 20° C ($T = 293$ K), which is a round number representative of typical laboratory temperatures. The saturation concentration at this temperature is $b_{\text{sat}} = 4.56$ mol kg^{-1}.[27] At no point was homogeneous nucleation observed in the simulations, even following lengthy MD test runs.[39] It is emphasized again that in this work on KCl, homogeneous nucleation is *not* of interest, since the real supersaturated solutions remain metastable for periods

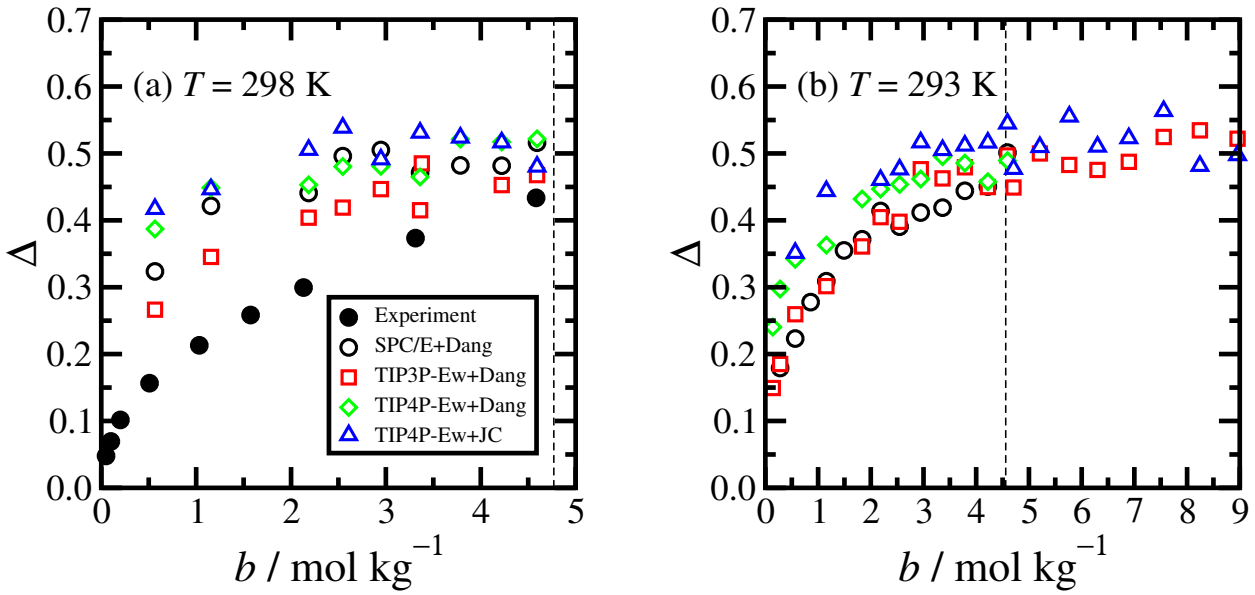

Figure 2: Deviation from the Nernst-Einstein relation measured by the parameter Δ, defined in eq 5. Results are shown from simulations with different models (unfilled symbols) and from experiment (filled symbols).[31,32,37,38] The vertical dashed lines mark the experimental saturation concentrations:[27] (a) $T = 298$ K, $b_{\mathrm{sat}} = 4.77$ mol kg^{-1}; (b) $T = 293$ K, $b_{\mathrm{sat}} = 4.56$ mol kg^{-1}.

of up to months.

The partial radial distribution functions (RDFs) $g_{\alpha\beta}(r)$ ($\alpha,\beta = +,-$ corresponding to $\mathrm{K}^+, \mathrm{Cl}^-$) are shown at selected concentrations for the TIP3P-Ew+Dang and TIP4P-Ew+JC models in Figure 3. The cation-anion function $g_{+-}(r)$ shows a very strong first peak due to the association of the ions, which is to be examined in more detail in Section 3.3. The positions of the first maximum and minimum in $g_{+-}(r)$ are quite insensitive to concentration, remaining in the regions of $r \simeq 3.2$ Å and $r \simeq 4.1$ Å, respectively, for the TIP3P-Ew+Dang model, and slightly smaller values for the TIP4P-Ew+JC model. The first maxima of $g_{++}(r)$ and $g_{--}(r)$ are in the range $r = 4.5$–5.0 Å, with the difference between the peak positions decreasing with increasing concentration.

Structure factors have been calculated by explicit evaluation of the Fourier components of the density of species $\alpha = +,-$

$$\rho_\alpha(\boldsymbol{k}) = \sum_{j=1}^{N_\alpha} e^{-i\boldsymbol{k}\cdot\boldsymbol{r}_j} \tag{6}$$

where the sum is restricted to the N_α particles of type α, and $\boldsymbol{k}$ is a wavevector that is commensurate with the periodic boundary conditions on the simulation cell. The partial structure factors are

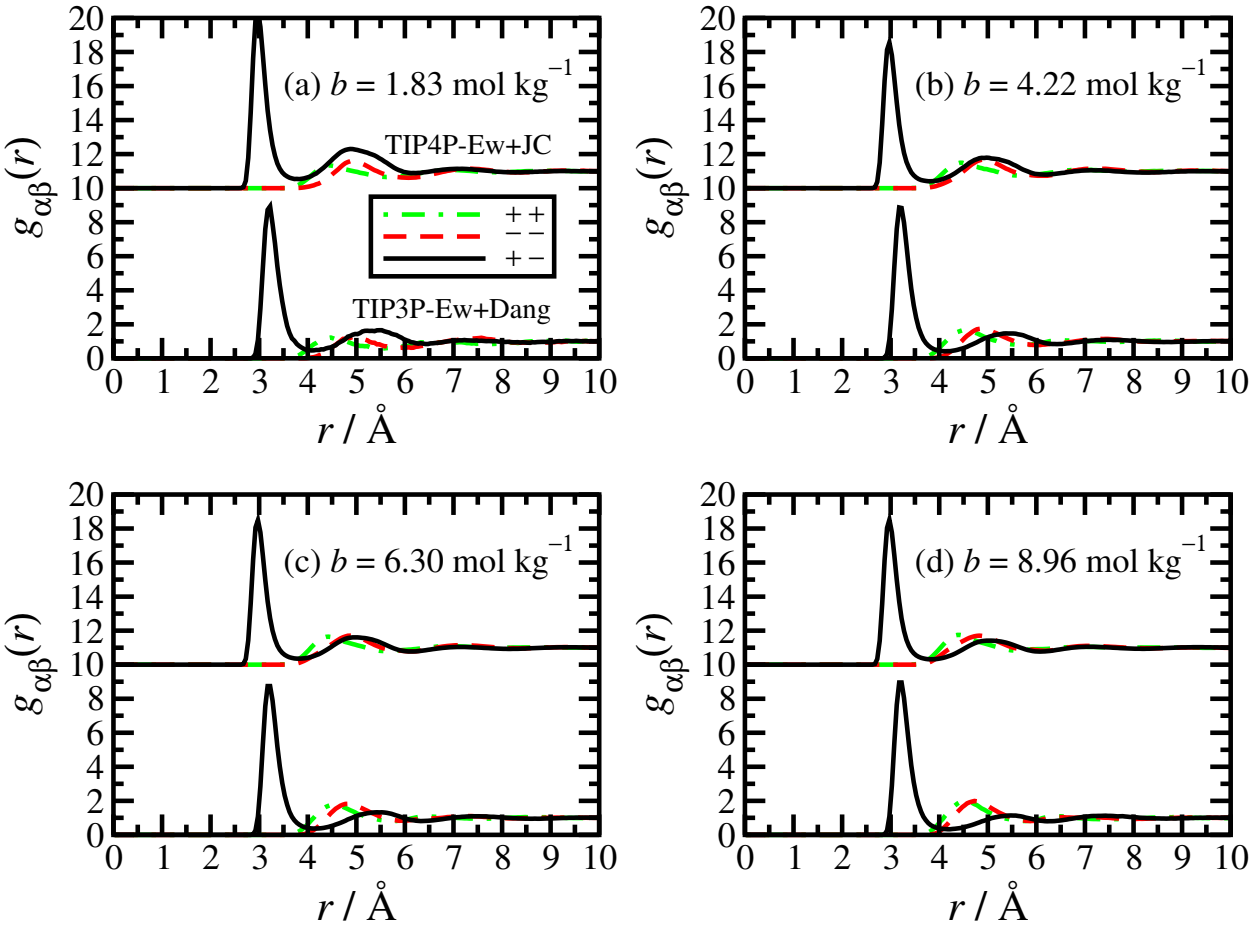

Figure 3: The partial radial distribution functions $g_{\alpha\beta}(r)$ ($\alpha = +,-$ corresponding to K^+, Cl^-) at $T = 293$ K: (a) $b = 1.83$ mol kg^{-1}; (b) $b = 4.22$ mol kg^{-1}; (c) $b = 6.30$ mol kg^{-1}; (d) $b = 8.96$ mol kg^{-1}. Data are shown for the TIP3P-Ew+Dang model, and the TIP4P-Ew+JC model (shifted up by 10 units for clarity).

defined by[36]

$$S_{\alpha\beta}(\boldsymbol{k}) = \frac{1}{N}\langle \rho_\alpha(\boldsymbol{k})\rho_\beta(-\boldsymbol{k})\rangle. \tag{7}$$

Since the solution is isotropic, structure factors with equal $k = |\boldsymbol{k}|$ were averaged. As defined, $S_{++}(k)$ and $S_{--}(k)$ tend to $\frac{1}{2}$ at large k, while $S_{+-}(k)$ tends to zero. The number-number structure factor $S_{NN}(\boldsymbol{k})$, number-charge structure factor $S_{NZ}(\boldsymbol{k})$, and charge-charge structure factor $S_{ZZ}(\boldsymbol{k})$ are given by[36]

$$\begin{aligned}
S_{NN}(\boldsymbol{k}) &= \frac{1}{N}\langle \rho_N(\boldsymbol{k})\rho_N(-\boldsymbol{k})\rangle = S_{++}(\boldsymbol{k}) + S_{--}(\boldsymbol{k}) + 2S_{+-}(\boldsymbol{k}) && (8)\\
S_{NZ}(\boldsymbol{k}) &= \frac{1}{N}\langle \rho_N(\boldsymbol{k})\rho_Z(-\boldsymbol{k})\rangle = S_{++}(\boldsymbol{k}) - S_{--}(\boldsymbol{k}) && (9)\\
S_{ZZ}(\boldsymbol{k}) &= \frac{1}{N}\langle \rho_Z(\boldsymbol{k})\rho_Z(-\boldsymbol{k})\rangle = S_{++}(\boldsymbol{k}) + S_{--}(\boldsymbol{k}) - 2S_{+-}(\boldsymbol{k}) && (10)
\end{aligned}$$

where $\rho_N(\boldsymbol{k}) = \rho_+(\boldsymbol{k}) + \rho_-(\boldsymbol{k})$ and $\rho_Z(\boldsymbol{k}) = \rho_+(\boldsymbol{k}) - \rho_-(\boldsymbol{k})$ are the Fourier components of the total number and charge densities, respectively. Figure 4 shows examples of the partial structure factors $S_{\alpha\beta}(k)$ and the number-and-charge structure factors $S_{AB}(k)$ $(A,B = N,Z)$ at two concentrations. Firstly, $S_{+-}(k)$ shows the most structure at higher wavevectors due to the strong association of cations and anions. Given the intense and narrow first peak in $g_{+-}(r)$, and the Fourier transform that links $g_{\alpha\beta}(r)$ and $S_{\alpha\beta}(k)$,[36] the structure factor is expected to be roughly

$$S_{+-}(k) \propto \int_0^\infty r^2\left[g_{+-}(r) - 1\right]\frac{\sin kr}{kr}\mathrm{d}r \simeq \frac{C\sin kR}{kR} \tag{11}$$

where R is the position of the first peak in $g_{+-}(r)$. Fitting this function to $S_{+-}(k)$ gives $R \simeq 3.3$ Å at both concentrations, which corresponds well with the peak positions in $g_{+-}(r)$. The first peaks in $S_{++}(k)$ and $S_{--}(k)$ are at around $k \simeq 1.5$ Å^{-1}, which corresponds to a real-space distance $R \simeq 2\pi/k = 4.2$ Å, as per the corresponding RDFs. The number-number structure factor $S_{NN}(k)$ shows a low-k feature which could be mistaken as signaling intermediate-range order, but in fact this just comes from the low-k behavior of $S_{+-}(k)$ arising from the cation-anion association.

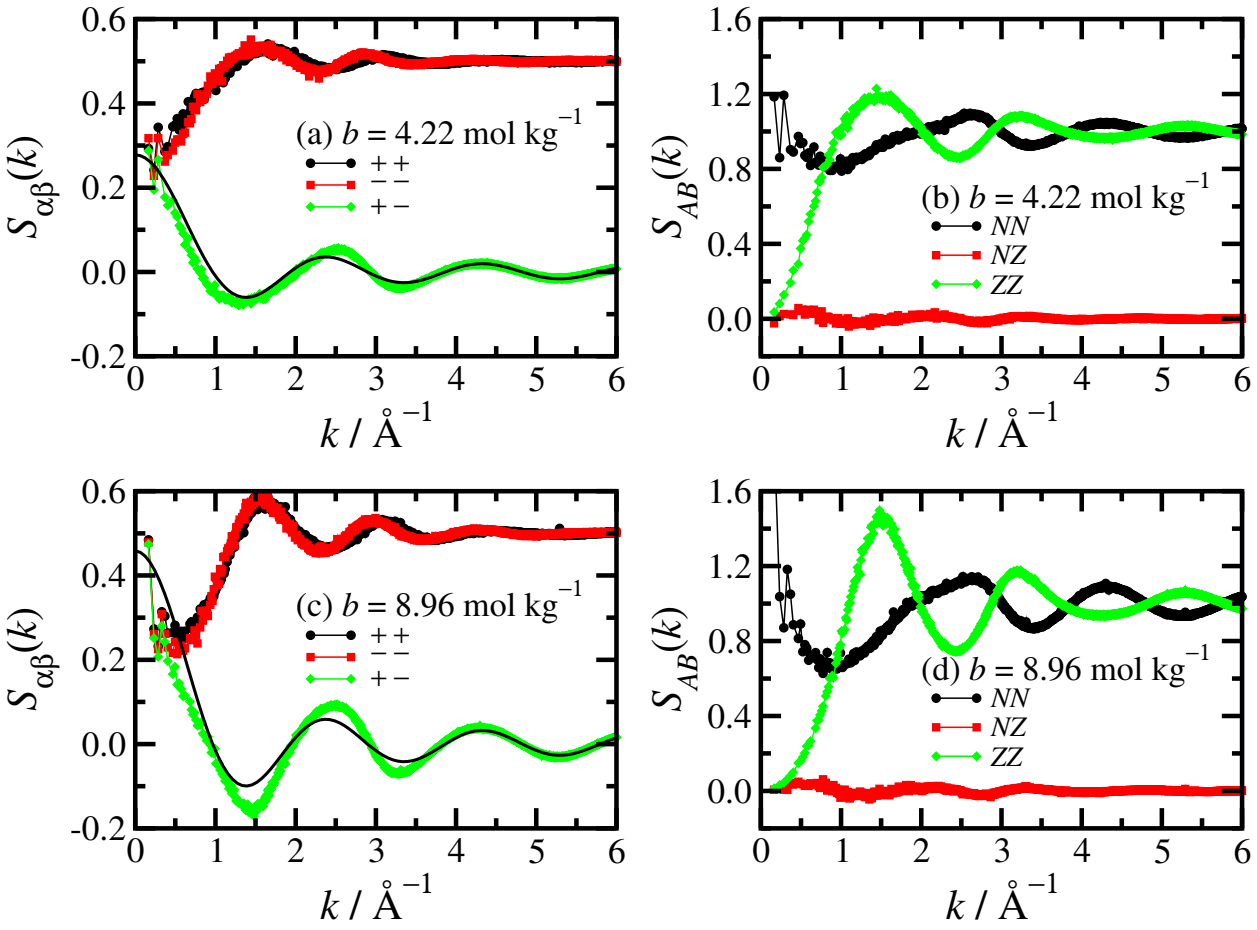

Figure 4: Partial structure factors $S_{\alpha\beta}(k)$ and number-and-charge structure factors $S_{AB}(k)$ for the TIP3P-Ew+Dang model at $T = 293$ K: (a) and (b) $b = 4.22$ mol kg^{-1}; (c) and (d) $b = 8.96$ mol kg^{-1}. In a and c, the solid line is a fit to eq 11.

3.3 Degree of ion association, residence time, and cluster distribution

Any two ions *of opposite charge* are considered clustered if the distance between them is less than a cut-off distance r_c (the Stillinger criterion[40]). The cut-off distance $r_c = 4.1$ Å was set as the position of the first local minimum in the cation-anion radial distribution function $g_{+-}(r)$. Figure 5 shows the fraction of associated ions (the degree of association α), and the fractions of ions bound in neutral and charged clusters, according to the Stillinger criterion for two models – TIP3P-Ew+Dang and TIP4P-Ew+JC. Despite the differences in density, molar conductivity, and ion self-diffusion coefficients shown in Figure 1, the different models give similar values of α. For a given concentration, the TIP4P-Ew+JC model gives a slightly smaller value of α than the TIP3P-Ew+Dang model, possibly due to the smaller cation-anion interaction parameter ($\varepsilon_{+-} \simeq 0.0571$ kcal mol^{-1} versus 0.100 kcal mol^{-1}) obtained from the mixing rules. Neutral clusters dominate at low concentrations, while the proportion of charged clusters grows with increasing concentration. This is a characteristic feature of association in ionic liquids:[41,42] at very low concentrations, strongly interacting ions primarily form neutral dimers, tetramers, hexamers, etc.

The residence time of an ion in the associated state was explored using the normalized correlation function

$$C_\theta(t) = \frac{\langle \theta(t)\theta(0)\rangle}{\langle \theta(0)\theta(0)\rangle} \tag{12}$$

where $\theta(t) = 1$ if the ion was associated continuously in the time interval $0 \leq t' \leq t$ and $\theta(0) = 0$ otherwise. As defined, $C_\theta(0) = 1$, and $\langle \theta(0)\theta(0)\rangle$ is equal to the degree of ion association. Figure 6 shows results for the TIP3P-Ew+Dang and TIP4P-Ew+JC models. Figure 6a shows examples of $C_\theta(t)$ from the TIP3P-Ew+Dang model at selected concentrations; the correlation function decays more slowly with increasing concentration. A residence time can be computed from the expression

$$t_{\text{res}} = \int_0^\infty C_\theta(t)\ \mathrm{d}t. \tag{13}$$

The residence time as a function of concentration is shown in Figure 6b. The results for the TIP3P-Ew+Dang and TIP4P-Ew+JC models are practically identical, and show that the residence

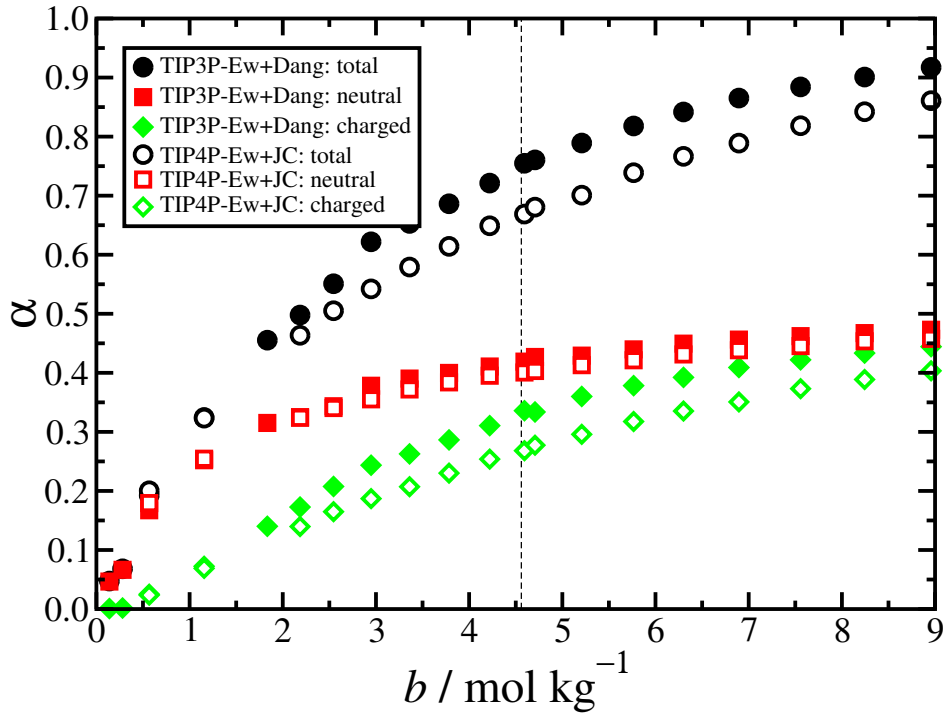

Figure 5: The degree of ion association α, and the fractions of ions in neutral and charged clusters, as functions of concentration at $T = 293$ K from the Stillinger criterion with $r_c = 4.1$ Å. The filled symbols are for the TIP3P-Ew+Dang model, and the unfilled symbols are for the TIP4P-Ew+JC model. The vertical dashed line marks the experimental saturation concentration $b_{sat} = 4.56$ mol kg^{-1} at $T = 293$ K.[27]

time increases from 5–10 ps at low concentration, to about 40 ps at the experimental saturation concentration. The residence time continues to increase in the supersaturated-solution regime, up to around 100 ps.

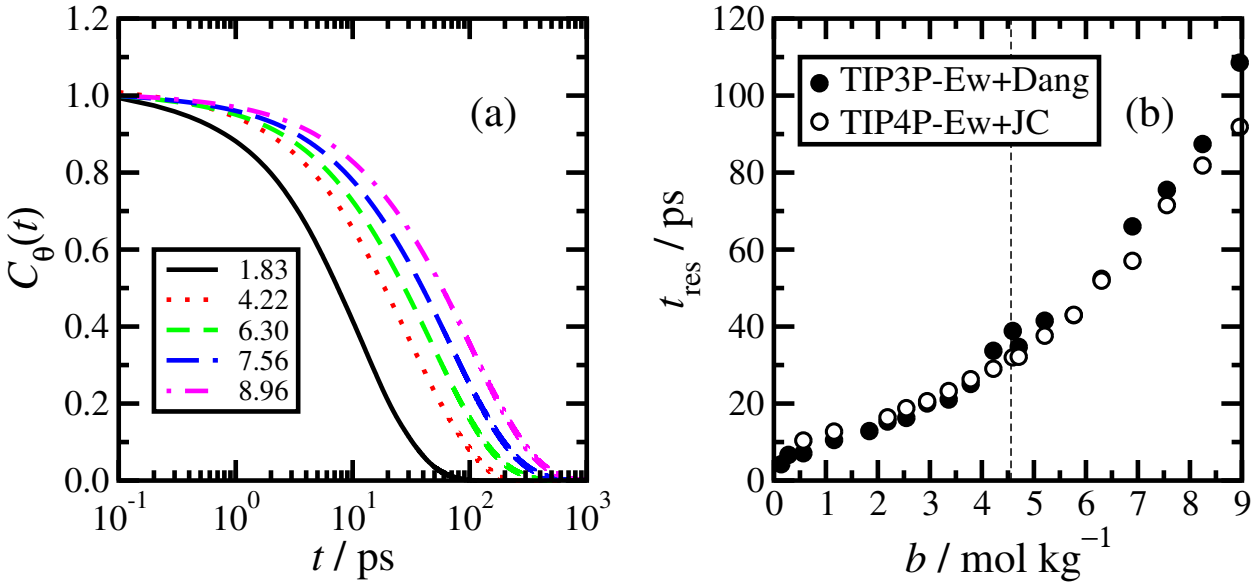

Figure 6: (a) The ion association correlation function $C_\theta(t)$ at selected concentrations (shown in mol kg^{-1}) for the TIP3P-Ew+Dang model at $T = 293$ K. (b) The residence time, t_{res}, computed from eq 13. Results are shown for the TIP3P-Ew+Dang model (filled circles) and the TIP4P-Ew+JC model (open circles). The vertical dashed line marks the experimental saturation concentration $b_{sat} = 4.56$ mol kg^{-1} at $T = 293$ K.[27]

Figure 7 shows simulation snapshots of the ions colored according to residence time, at concentrations of $b = 1.83$, 4.22, 6.30, and 8.96 mol kg^{-1}. To produce these figures, 25 ps simulations were initiated from well-equilibrated configurations, and the time that each ion remained in a cluster was calculated. Ions that are unclustered at the start are assigned a residence time $t_{res} = 0$ and colored red; ions that remain clustered for the whole 25 ps are colored blue, but of course Figure 6b shows that much longer residence times are possible. The 25 ps window was chosen to give a good spread of colors at the highest concentration. As concentration is increased, the proportion of ions with long residence times increases. At the highest concentration ($b = 8.96$ mol kg^{-1}) these long-residence-time ions appear to be concentrated in to a single extended amorphous cluster, while ions on the periphery have shorter residence times, and those beyond the periphery have the shortest residence times. In essence, this is a kind of dynamical cluster formation, where the criterion for

clustering is based on residence time. This isn't pursued further here, but instead structural cluster formation is considered next.

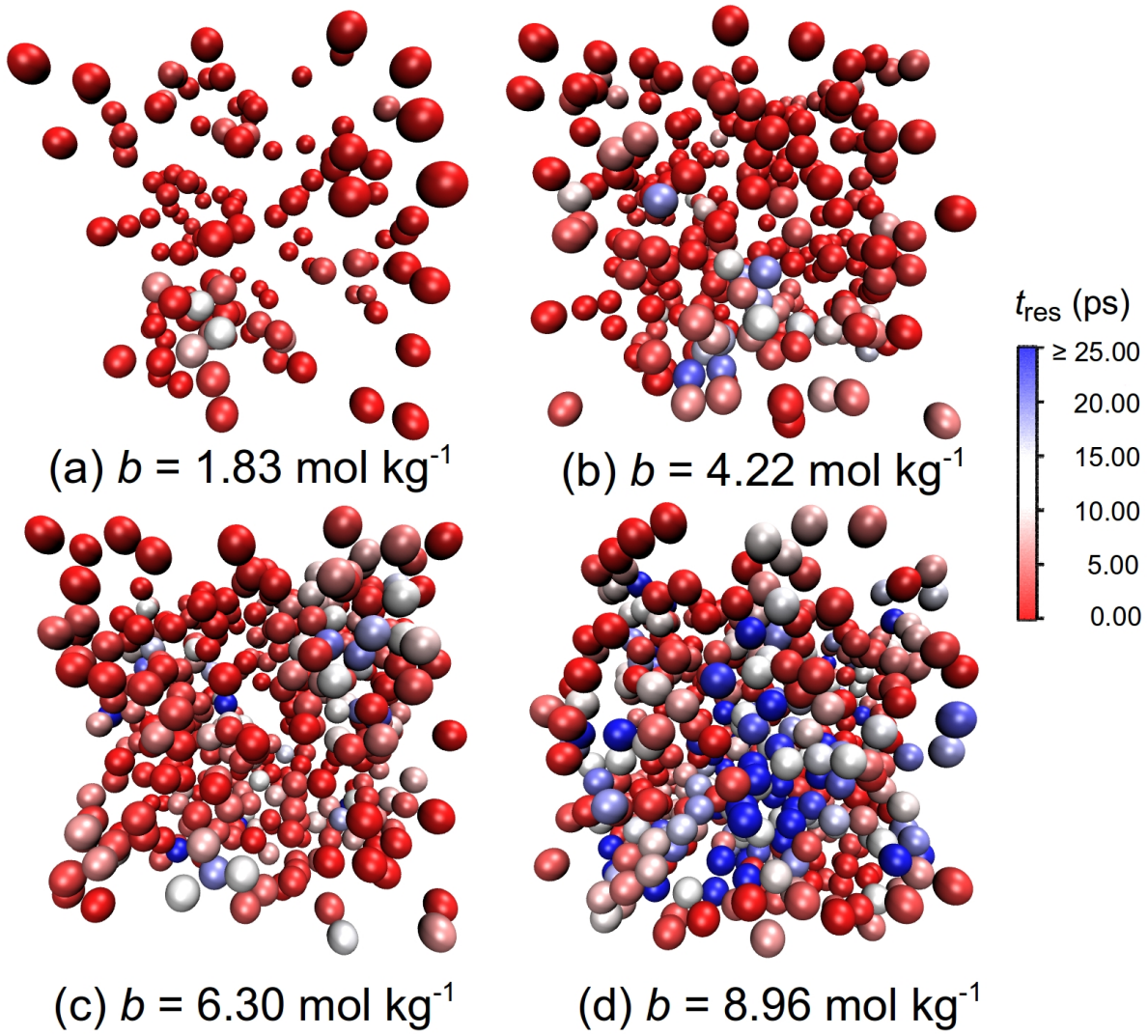

Figure 7: Snapshots where ions are colored according to the cluster residence time t_{res} over a simulation of 25 ps. Ions that are unclustered at the start are assigned a residence time $t_{res} = 0$ and colored red; ions that remain clustered for the whole 25 ps are colored blue. Figure 6b shows that much longer residence times are possible.

Given the clustering criterion for any pair of oppositely charged ions, it is possible to partition a configuration of N ions in to a set of disjoint clusters. The probability distribution p_n of cluster size n (or the fraction of all clusters that are of size n) is shown in Figure 8a. For concentrations up to $b = 6.90$ mol kg^{-1}, p_n decays monotonically with n until n approaches the total number of ions

in the box. For concentrations of $b = 7.56$ mol kg^{-1} and higher, a second peak appears. This is a finite-size effect due to artificial stabilization of system-spanning clusters by the periodic boundary conditions. This was determined by carrying out a single 10 ns run on a much larger system with 2000 KCl and 12000 H_2O, giving a molality of 9.25 mol kg^{-1} and a KCl mass percentage of 40.8%. Figure 8b compares the cluster distribution of this system with that of the original system at $b = 8.96$ mol kg^{-1}. Clearly, the measured probability distributions are only consistent up to $n \simeq 10^2$, and in the larger system, the peak corresponding to system-spanning clusters is comparable to the total number of ions. The mean $\langle n \rangle$ and standard deviation σ_n of the cluster-size distribution are shown in Figure 8c and d, respectively.

3.4 Hydration

Although the focus here is on ion association and the related residence times, a related question is how long a water molecule spends as a hydrating species. The water-ion partial radial distribution functions at low and high salt concentrations are shown in Figure 9a. There is very little variation with concentration. The Cl–H and K–O functions show that the first hydration shells of the anions and cations extend out to 2.9 Å and 3.6 Å, respectively. The average numbers of water molecules in the first hydration shells of the cations and anions are reported in Table 2. These decrease slightly with increasing ion concentration due to the formation of amorphous ion clusters that remain at least partially hydrated.

A correlation function equivalent to that in eq 12 was calculated with $\theta(t) = 1$ if a water molecule was in the first hydration shell of at least one ion continuously in the time interval $0 \leq t' \leq t$ and $\theta(0) = 0$ otherwise. This function was measured separately for hydration of cations only, anions only, and any ions. The associated residence times (eq 13) are shown in Figure 9b. Firstly, at low concentration, the cation, anion, and any-ion times are all about 3–4 ps because a water molecule may only hydrate one ion at a time. Secondly, at high concentration, the any-ion time is roughly the sum of the cation and anion times, because a water molecule can be shared between the hydration shells of different types of ion. Finally, for a given concentration, all of the hydration

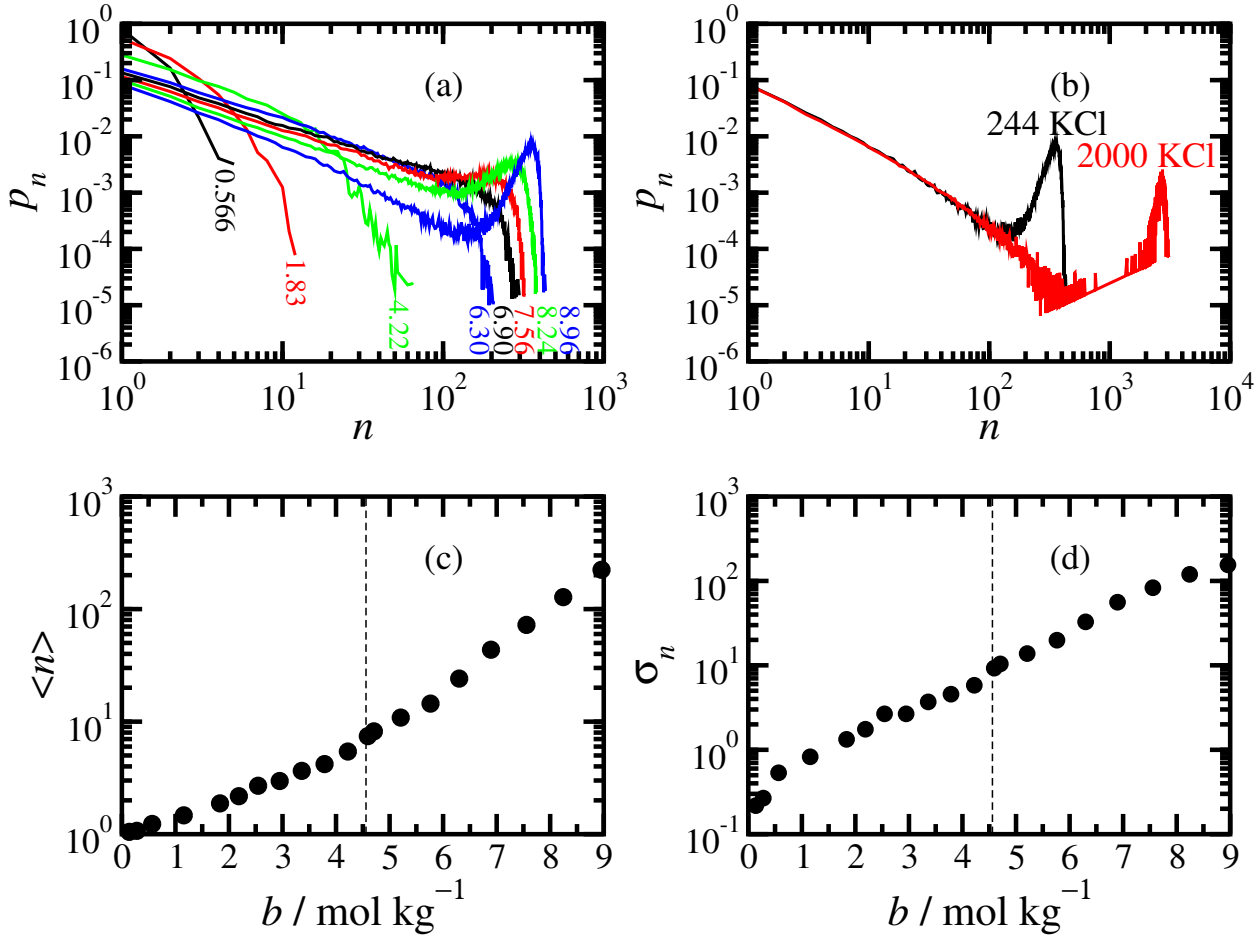

Figure 8: The cluster probability distribution, $p(n)$, and associated averages for the TIP3P-Ew+Dang model at $T = 293$ K. (a) $p(n)$ at concentrations of, from left to right, $b = 0.566$, 1.83, 4.22, 6.30, 6.90, 7.56, 8.24, and 8.96 mol kg^{-1}. (b) $p(n)$ from simulations with 244 KCl and 1512 H_2O ($b = 8.96$ mol kg^{-1}), and 2000 KCl and 12000 H_2O ($b = 9.25$ mol kg^{-1}). (c) Mean cluster size $\langle n \rangle$ as a function of concentration. (d) Standard deviation of the cluster size, $\sigma_n = (\langle n^2 \rangle - \langle n \rangle^2)^{1/2}$ as a function of concentration. In c and d, the vertical dashed lines mark the experimental saturation concentration $b_{\text{sat}} = 4.56$ mol kg^{-1} at $T = 293$ K.[27]

residence times ($\leq$ 18 ps) are significantly shorter than the ion-association residence time shown in Figure 6b. It is therefore appropriate to think of the ion clusters as remaining relatively intact while water molecules are shuttling in and out of the hydration shells of the constituent ions. This suggests that, in a two-step NPLIN scenario, the relaxation dynamics of the ions controls one or both of the steps.

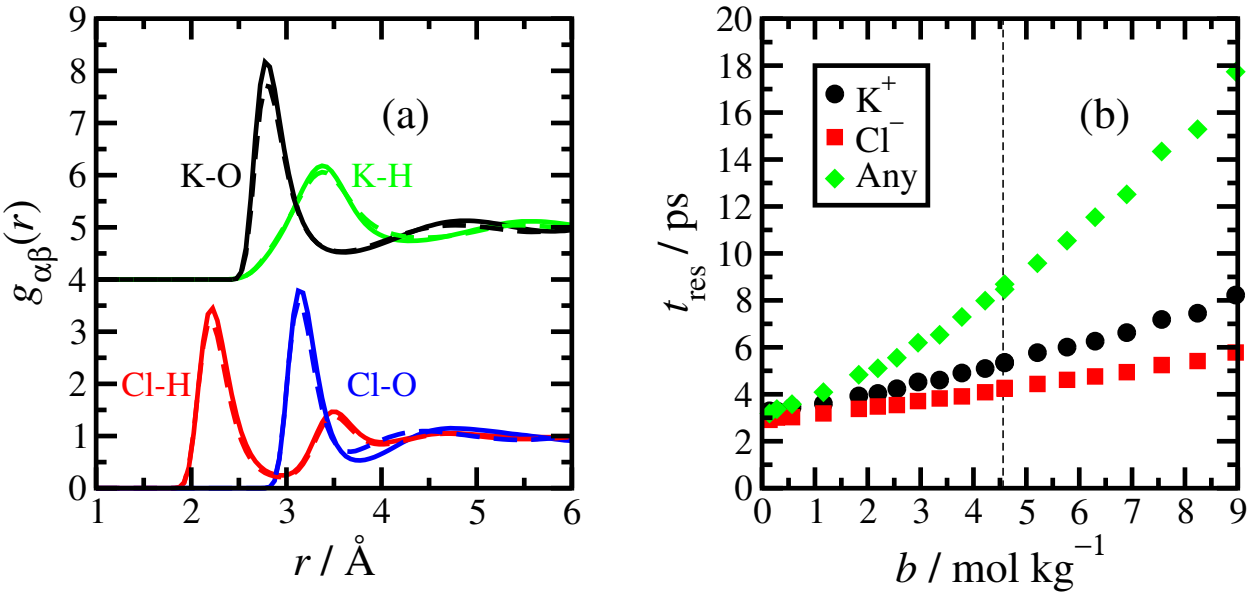

Figure 9: (a) Water-ion partial radial distribution functions at low concentration (b = 1.83 mol kg^{-1}, solid lines) and at high concentration (b = 8.96 mol kg^{-1}, dashed lines) for the TIP3P-Ew+Dang model at T = 293 K. The K–O and K–H results are shifted up by 4 units for clarity. (b) Hydration residence times for K^+ ions (circles), Cl^- ions (squares), and any ions (diamonds). The vertical dashed line marks the experimental saturation concentration b_{sat} = 4.56 mol kg^{-1} at T = 293 K.[27]

3.5 Space-dependent self diffusion

The self-intermediate scattering function $F_s(\boldsymbol{k},t)$[36,43] was calculated in order to investigate ion motion in more detail. In the current case, this is defined by

$$F_s(\boldsymbol{k},t) = \frac{1}{N}\sum_{j=1}^{N}\left\langle e^{-i\boldsymbol{k}\cdot[\boldsymbol{r}_j(t)-\boldsymbol{r}_j(0)]}\right\rangle \tag{14}$$

where the sum is over all ions, and results for wavevectors with equal $k = |\boldsymbol{k}|$ are averaged. This function represents the contribution of a single particle to each of the time-dependent structure factors $S_{NN}(\boldsymbol{k},t) = N^{-1}\langle\rho_N(\boldsymbol{k},t)\rho_N(-\boldsymbol{k},0)\rangle$ and $S_{ZZ}(\boldsymbol{k},t) = N^{-1}\langle\rho_Z(\boldsymbol{k},t)\rho_Z(-\boldsymbol{k},0)\rangle$. At short times, $F_s(k,t) \approx \exp(-\frac{1}{2}k^2v_0^2t^2)$ where $v_0^2 = k_BT/m$ is the mean-square velocity of a particle.[43] It is convenient to focus attention on the long-time, non-trivial behavior of $F_s(k,t)$ by plotting it for times $t \geq t_0$, where t_0 is a time beyond the free-particle regime.[44] Figure 10 shows the quantity $F_s(k,t)/F_s(k,t_0)$ at $k = 1.50$ Å^{-1} and 2.45 Å^{-1} corresponding to the primary peak positions in $S_{NN}(k)$ and $S_{ZZ}(k)$, respectively. Results are shown for a selection of concentrations from across the entire range, and at simulated times greater than $t_0 = 0.4$ ps for $k = 1.50$ Å^{-1} and $t_0 = 0.2$ ps for $k = 2.45$ Å^{-1}. In Figure 10a and b, the simulation results are fitted with the conventional Fickian-dynamics expression (valid at low wavevectors and long times)

$$F_s(k,t) = F_s(k,t_0)e^{-(t-t_0)/\tau(k)} \quad t \geq t_0 \tag{15}$$

where $\tau(k) = 1/Dk^2$, and D is the self-diffusion coefficient. (The time origin t_0 was in fact chosen to give the minimum weighted sum of the squared residuals in the fits.) At low concentrations $b < 4$ mol kg^{-1}, the results at the lower wavevector can be fitted adequately with the normal exponential expression: the deviations at higher wavevector are expected as the hydrodynamic picture breaks down. At higher concentrations, however, there are significant deviations between all of the results and the fits. It was found that a stretched exponential gave superior fits over the whole range of concentrations and at both wavevectors:

$$F_s(k,t) = F_s(k,t_0)e^{-[(t-t_0)/\tau(k)]^\beta} \quad t \geq t_0. \tag{16}$$

Figure 10c and d show the simulation results again, along with the stretched-exponential fits; the agreement is now essentially perfect. Stretched-exponential behavior in the self-intermediate scattering function is often associated with glassy behavior,[44] and in some simple models it can be shown explicitly to arise from the presence of distinct timescales for the first 'step' of a particle and

subsequent 'steps' due to the influence of neighbors.[45] No claim is being made here about glassy behavior in aqueous electrolyte solutions under ambient conditions, but the stretched-exponential decay of $F_s(k,t)$ does perhaps suggest some sort of complex, single-particle dynamics influenced by cooperative motion within ion clusters. Incidentally, fitting a sum of two normal exponentials (perhaps corresponding to 'associated' and 'dissociated' ions) gives marginally better fits than one exponential, but nowhere near as good as the stretched-exponential function.

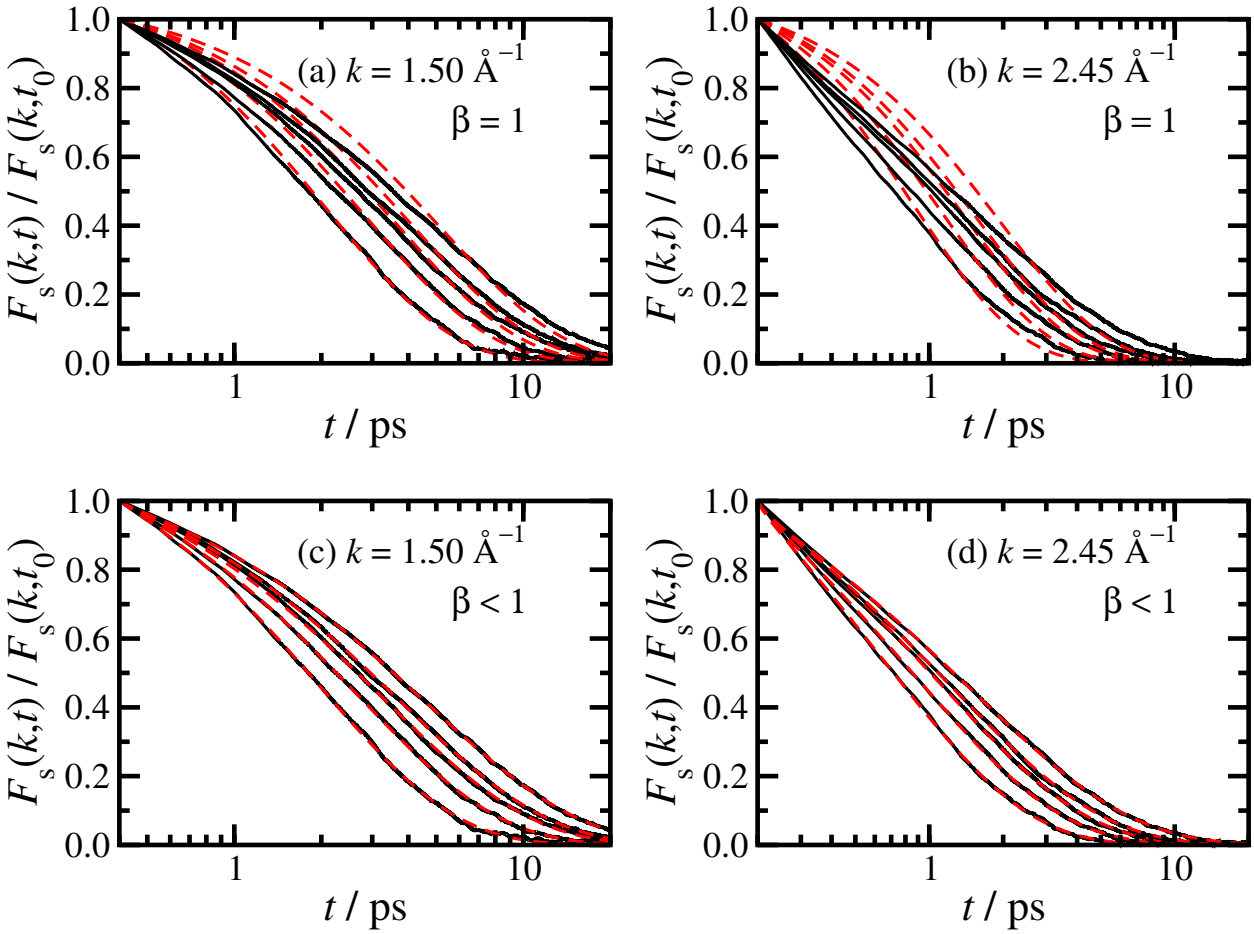

Figure 10: Self-intermediate scattering functions $F_s(k,t)$ for the TIP3P-Ew+Dang model at T = 293 K and with concentrations of, from left to right in each panel, b = 1.83, 4.22, 6.30, 7.56, and 8.96 mol kg^{-1}: (a) and (c) k = 1.50 Å^{-1} (with t_0 = 0.4 ps); (b) and (d) k = 2.45 Å^{-1} (with t_0 = 0.2 ps). In a and b the results are fitted with a normal exponential (eq 15). In c and d the results are fitted with a stretched exponential (eq 16). Simulation results are shown as solid lines, and the fits are shown as dashed lines.

The timescales $\tau(k)$ associated with the normal-exponential and stretched-exponential fits are shown in Figure 11. Figure 11a shows $\tau(k)$ from eq 15. Assuming Fickian dynamics, the self-diffusion coefficient is $D = 1/\tau k^2$. This quantity is shown in Figure 11b, along with the cation and anion self-diffusion coefficients calculated at $T = 293$ K using eq 3. The fact that all of the data are consistent with one another is due to the similarity between the cation and anion self-diffusion coefficients, and that τ follows the Fickian scaling k^{-2}. This is surprising at high concentrations, given the discrepancies in the fits to eq 15. The timescales extracted using the stretched-exponential fit (eq 16) are shown in Figure 11c and are not markedly different from those from the Fickian fit. Figure 11d shows the apparent values of the exponent β for each wavevector. For the lower wavevector, β tends to unity at low concentration, presumably due to the onset of independent ion migration. There is currently no theoretical explanation for the observed dependence of β on b.

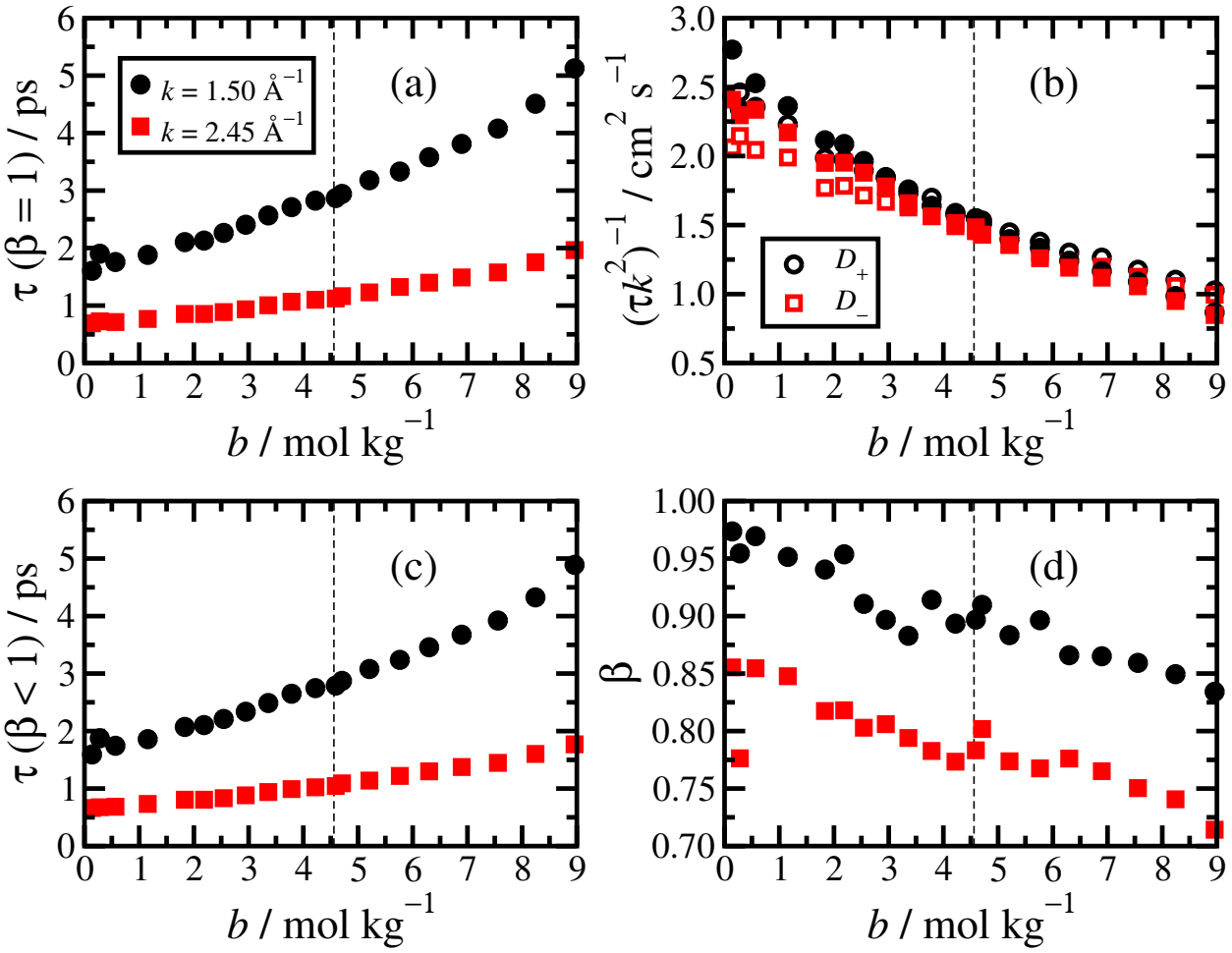

Figure 11: Relaxation time τ, apparent self-diffusion coefficient $(\tau k^2)^{-1}$, and stretched-exponential parameter β for the TIP3P-Ew+Dang model at $T = 293$ K, obtained from fits to $F_s(k,t)$ at $k = 1.50$ Å^{-1} (filled symbols) and $k = 2.45$ Å^{-1} (filled squares). (a) τ from a normal-exponential fit (eq 15). (b) $(\tau k^2)^{-1}$ from a normal-exponential fit, compared to the actual cation and anion self-diffusion coefficients (D_+ and D_-, unfilled circles and unfilled squares, respectively) calculated using the Green-Kubo formula (eq 3). (c) and (d) τ and β from a stretched-exponential fit (eq 16). The vertical dashed lines mark the experimental saturation concentration $b_{sat} = 4.56$ mol kg^{-1} at $T = 293$ K.[27]

4 Conclusions

In this work, the structure and dynamics of potassium chloride in aqueous solution were examined using molecular dynamics computer simulations. The motivation for the work was the observation that nonphotochemical laser-induced nucleation in supersaturated KCl solutions is dependent on the duration of the laser pulse: if the laser pulse is 5 ps or less, then no nucleation is observed; if the laser pulse is longer than 100 ps, then nucleation is observed. The aim of the current work was to see if there is any structural reorganization of solute clusters on the intermediate timescale (5–100 ps). Note that homogeneous nucleation is not of interest here, since real supersaturated KCl solutions remain unnucleated for periods of up to months. First, various molecular models were tested against basic experimental data (mass density, molar conductivity, and ion self-diffusion coefficients). The TIP3P water model[21,22] in combination with the KCl parameters obtained by Dang[24] were selected for further study, but spot checks were made for a more contemporary model (the TIP4P water model[21,23] with KCl parameters optimized by Joung and Cheatham[25,26]). Next, radial distribution functions and structure factors were computed across a full range of KCl concentrations, up to well above the experimental saturation concentration. The major structural motif is the strong association of cations and anions. Based on this motif, the majority of ions are found to be associated at concentrations above saturation. The lifetime of an ion in the associated state increases rapidly with increasing concentration, and above saturation it exceeds 40 ps, and is well within the intermediate experimental timescale given above. The residence time of a water molecule in the first hydration shell of an ion is considerably shorter, being only 18 ps even at the highest ion concentration. Hence, it is likely that associated ions control the relevant dynamics in solution. The ion cluster-size distribution shows a monotonic growth in the mean cluster size and the standard deviation, but at very high concentrations, finite-size effects lead to artificial stabilization of system-spanning clusters. The self-intermediate scattering function of the ions shows non-trivial, stretched-exponential relaxation above saturation, and regular exponential (Fickian) relaxation below saturation. This points to some sort of complex single-particle dynamics, possibly influenced by cooperative motion within ion clusters. The overall conclusion is that the ion

dynamics in supersaturated KCl solutions is complex, and that there are timescales (such as the ion-association lifetime) that match with the threshold laser-pulse duration for nonphotochemical laser-induced nucleation to occur. If pre-existing solute clusters have to rearrange and/or grow during the laser pulse for nucleation to occur, then perhaps it is necessary (but probably not sufficient) for the pulse to at least exceed the ion-association lifetime, over which period ions can leave and join a cluster.

Acknowledgments

This research was supported by the Engineering and Physical Sciences Research Council through the provision of a studentship to J.O.S. The authors acknowledge helpful discussions with Dr Julien Michel (Edinburgh).

Notes and References

(1) Robinson, R. A.; Stokes, R. H. *Electrolyte Solutions*, 2nd ed.; Butterworths: London, 1959.

(2) Verwey, E. J. W.; Overbeek, J. T. G. *Theory of the Stability of Lyophobic Colloids*; Elsevier: Amsterdam, 1948.

(3) Bard, A. J.; Faulkner, L. R. *Electrochemical Methods: Fundamentals and Applications*, 2nd ed.; John Wiley & Sons, Inc.: New York, 2001.

(4) Garetz, B. A.; Aber, J. E.; Goddard, N. L.; Young, R. G.; Myerson, A. S. Nonphotochemical, Polarization-Dependent, Laser-Induced Nucleation in Supersaturated Aqueous Urea Solutions. *Phys. Rev. Lett.* **1996**, *77*, 3475–3476.

(5) Garetz, B. A.; Matic, J.; Myerson, A. S. Polarization Switching of Crystal Structure in the Nonphotochemical Light-Induced Nucleation of Supersaturated Aqueous Glycine Solutions. *Phys. Rev. Lett.* **2002**, *89*, 175501.

(6) Sun, X.; Garetz, B. A.; Myerson, A. S. Supersaturation and Polarization Dependence of Polymorph Control in the Nonphotochemical Laser-Induced Nucleation (NPLIN) of Aqueous Glycine Solutions. *Cryst. Growth Des.* **2006**, *6*, 684–689.

(7) Alexander, A. J.; Camp, P. J. Single Pulse, Single Crystal Laser-Induced Nucleation of Potassium Chloride. *Cryst. Growth. Des.* **2009**, *9*, 958–963.

(8) Duffus, C.; Camp, P. J.; Alexander, A. J. Spatial Control of Crystal Nucleation in Agarose Gel. *J. Am. Chem. Soc.* **2009**, *131*, 11676–11677.

(9) Ward, M. R.; Ballingall, I.; Costen, M. L.; McKendrick, K. G.; Alexander, A. J. Nanosecond Pulse Width Dependence of Nonphotochemical Laser-Induced Nucleation of Potassium Chloride. *Chem. Phys. Lett.* **2009**, *481*, 25–28.

(10) Fang, K.; Arnold, S.; Garetz, B. A. Nonphotochemical Laser-Induced Nucleation in Levitated Supersaturated Aqueous Potassium Chloride Microdroplets. *Cryst. Growth Des.* **2014**, Article ASAP.

(11) Ward, M. R.; Alexander, A. J. Nonphotochemical Laser-Induced Nucleation of Potassium Halides: Effects of Wavelength and Temperature. *Cryst. Growth Des.* **2012**, *12*, 4554–4561.

(12) Erdemir, D.; Lee, A. Y.; Myerson, A. S. Nucleation of Crystals from Solution: Classical and Two-Step Models. *Acc. Chem. Res.* **2009**, *42*, 621–629.

(13) Vekilov, P. G. Nucleation. *Cryst. Growth Des.* **2010**, *10*, 5007–5019.

(14) Agarwal, V.; Peters, B. Solute Precipitate Nucleation: A Review of Theory and Simulation Advances. *Adv. Chem. Phys.* **2014**, *155*, 97–159.

(15) Chakraborty, D.; Patey, G. N. How Crystals Nucleate and Grow in Aqueous NaCl Solution. *J. Phys. Chem. Lett.* **2013**, *4*, 573–578.

(16) Chakraborty, D.; Patey, G. N. Evidence that Crystal Nucleation in Aqueous NaCl Solution Occurs by the Two-Step Mechanism. *Chem. Phys. Lett.* **2013**, *587*, 25–29.

(17) Giberti, F.; Tribello, G. A.; Parrinello, M. Transient Polymorphism in NaCl. *J. Chem. Theory. Comput.* **2013**, *9*, 2526–2530.

(18) Alexander, A. J. Deep Ultraviolet and Visible Crystalloluminescence of Sodium Chloride. *J. Chem. Phys.* **2012**, *136*, 064512.

(19) Sellner, B.; Valiev, M.; Kathmann, S. M. Charge and Electric Field Fluctuations in Aqueous NaCl Electrolytes. *J. Phys. Chem. B* **2013**, *117*, 10869–10882.

(20) Berendsen, H. J. C.; Grigera, J. R.; Straatsma, T. P. The Missing Term in Effective Pair Potentials. *J. Phys. Chem.* **1987**, *91*, 6269–6271.

(21) Jorgensen, W. L.; Chandrasekhar, J.; Madura, J. D.; Impey, R. W.; Klein, M. L. Comparison of Simple Potential Functions for Simulating Liquid Water. *J. Chem. Phys.* **1983**, *79*, 926–935.

(22) Price, D. J.; Brooks, C. L., III. A Modified TIP3P Water Potential for Simulation with Ewald Summation. *J. Chem. Phys.* **2004**, *121*, 10096–10103.

(23) Horn, H. W.; Swope, W. C.; Pitera, J. W.; Madura, J. D.; Dick, T. J.; Hura, G. L.; Head-Gordon, T. Development of an Improved Four-Site Water Model for Biomolecular Simulations: TIP4P-Ew. *J. Chem. Phys.* **2004**, *120*, 9665–9678.

(24) Dang, L. X. Mechanism and Thermodynamics of Ion Selectivity in Aqueous Solutions of 18-Crown-6 Ether: A Molecular Dynamics Study. *J. Am. Chem. Soc.* **1995**, *117*, 6954–6960.

(25) Joung, I. S.; Cheatham, T. E., III. Determination of Alkali and Halide Monovalent Ion Parameters for Use in Explicitly Solvated Biomolecular Simulations. *J. Phys. Chem. B* **2008**, *112*, 9020–9041.

(26) Joung, I. S.; Cheatham, T. E., III. Molecular Dynamics Simulations of the Dynamic and Energetic Properties of Alkali and Halide Ions Using Water-Model-Specific Ion Parameters. *J. Phys. Chem. B* **2009**, *113*, 13279–13290.

(27) Haynes, W. M. *CRC Handbook of Chemistry and Physics*, 94th ed.; CRC Press, Taylor & Francis Group: Boca Raton, FL, 2013.

(28) LAMMPS Molecular Dynamics Simulator. http://lammps.sandia.gov.

(29) Plimpton, S. J. Fast Parallel Algorithms for Short-Range Molecular Dynamics. *J. Comp. Phys.* **1995**, *117*, 1–19.

(30) Zhang, H.-L.; Han, S.-J. Viscosity and Density of Water + Sodium Chloride + Potassium Chloride Solutions at 298.15 K. *J. Chem. Eng. Data* **1996**, *41*, 516–520.

(31) Shedlovsky, T. The Electrolyte Conductivity of Some Uni-Univalent Electrolytes in Water at 25°. *J. Am. Chem. Soc.* **1932**, *54*, 1411–1428.

(32) Chambers, J. F.; Stokes, J. M.; Stokes, R. H. Conductances of Concentrated Aqueous Sodium and Potassium Chloride Solutions at 25°. *J. Phys. Chem.* **1956**, *60*, 985–986.

(33) Friedman, A. M.; Kennedy, J. W. The Self-Diffusion Coefficients of Potassium, Cesium, Iodide and Chloride Ions in Aqueous Solutions. *J. Am. Chem. Soc.* **1955**, *77*, 4499–4501.

(34) Mills, R. The Self-Diffusion of Chloride Ion in Aqueous Alkali Chloride Solutions at 25°. *J. Phys. Chem.* **1957**, *61*, 1631–1634.

(35) In plotting the experimental data, the conversion of molarity c (mol L^{-1}) to molality b (mol kg^{-1}) was determined by fitting to the molality-density data at $T = 298$ K given in ref 30: $b = b_1 c + b_2 c^2 + b_3 c^3$ with $b_1 = 1.0032(1)$, $b_2 = 0.0275(1)$, and $b_3 = 0.00203(2)$.

(36) Hansen, J.-P.; McDonald, I. R. *Theory of Simple Liquids*, 3rd ed.; Academic Press: London, 2006.

(37) Harned, H. S.; Nuttall, R. L. The Differential Diffusion Coefficient of Potassium Chloride in Aqueous Solutions. *J. Am. Chem. Soc.* **1949**, *71*, 1460–1463.

(38) Gosting, L. J. A Study of the Diffusion of Potassium Chloride in Water at 25° with the Gouy Interference Method. *J. Am. Chem. Soc.* **1950**, *72*, 4418–4422.

(39) This is in contrast to NaCl, where homogeneous nucleation is readily observed.[15,16] Some spot checks for NaCl(aq) at $T = 293$ K were carried out using TIP3P-Ew water and Dang's parameters for Na^+ ($\sigma = 2.584$ Å, $\varepsilon = 0.1000$ kcal mol^{-1}) and Cl^-.[24] The experimental solubility of NaCl is $b_{sat} = 6.14$ mol kg^{-1}.[27] Simulations at supersaturations $s \geq 0.95$ showed crystallization within runs of 10–20 ns.

(40) Stillinger, F. H., Jr.. Rigorous Basis of the Frenkel-Band Theory of Association Equilibrium. *J. Chem. Phys.* **1963**, *38*, 1486–1494.

(41) Caillol, J.-M.; Weis, J.-J. Free Energy and Cluster Structure in the Coexistence Region of the Restricted Primitive Model. *J. Chem. Phys.* **1995**, *102*, 7610–7621.

(42) Valeriani, C.; Camp, P. J.; Zwanikken, J. W.; van Roij, R.; Dijkstra, M. Ion Association in Low-Polarity Solvents. *Soft Matter* **2010**, *6*, 2793–2800.

(43) Boon, J.-P.; Yip, S. *Molecular Hydrodynamics*; Dover Publications, Inc.: New York, 1980.

(44) Sastry, S.; Debenedetti, P. G.; Stillinger, F. H. Signatures of Distinct Dynamical Regimes in the Energy Landscape of a Glass-Forming Liquid. *Nature* **1998**, *393*, 554–557.

(45) Berthier, L.; Chandler, D.; Garrahan, J. P. Length Scale for the Onset of Fickian Diffusion in Supercooled Liquids. *Europhys. Lett.* **2005**, *69*, 320–326.

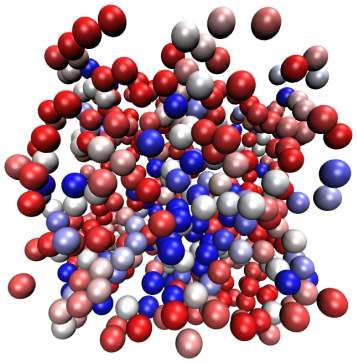

For Table of Contents Only